Materials Horizons

COMMUNICATION

View Article Online
View Journal | View Issue

Cite this: *Mater. Horiz.*, 2017, 4, 242

Received 15th November 2016,
Accepted 21st December 2016

DOI: 10.1039/c6mh00508j

www.rsc.li/materials-horizons

Integration of perovskite and polymer photoactive layers to produce ultrafast response, ultraviolet-to-near-infrared, sensitive photodetectors†

Liang Shen,‡[a] Yuze Lin,‡[a] Chunxiong Bao,[a] Yang Bai,[a] Yehao Deng,[a] Mengmeng Wang,[b] Tao Li,[c] Yongfeng Lu,[b] Alexei Gruverman,[c] Weiwei Li[d] and Jinsong Huang*[a]

Low-cost organic photodetectors have shown sensitivity levels comparable to those of inorganic photodetectors, but with response speeds generally limited to the megahertz range due to the low mobility of organic semiconductors. Here, we integrated organic–inorganic hybrid perovskite (OIHP) photoactive layers with low-bandgap organic bulk-heterojunction (BHJ) layers to produce a device that combined the advantages of the two types of photodetectors. Integrating methylammonium lead triiodide ($CH_3NH_3PbI_3$) with a low-bandgap BHJ layer extended the response of perovskite photodetectors to a wavelength of 1000 nanometers without deteriorating the responsivity and specific detectivity of either type of photodetector. The high mobility of charge carriers in $CH_3NH_3PbI_3$ allowed the constraints of the resistance–capacitance constant to be relieved so that the device response speed could be increased dramatically. A response time of five nanoseconds was measured for incident infrared light from the device with an active area of 0.1 square millimeters, which represents the state-of-the-art performance for organic-based photodetectors.

Conceptual insights

Solution-processable, polymer-based photodetectors have achieved responses to a wide spectrum of light, from the ultraviolet (UV) to the near infrared (NIR). However, the low mobility of most polymeric materials and the large resistance–capacitance (RC) time constant have limited the device response speed to the MHz range. Here we demonstrated that inserting perovskite as the charge-transport layer in polymeric photodetectors could alleviate the restriction of the RC constant, and was found to enhance the response speed of the polymeric photodetectors. A response time of 5 ns to 800 nm-wavelength NIR light was recorded from the hybrid device, and represents the state-of-the-art performance for organic-based photodetectors. In addition, the inclusion of the lower-bandgap polymers in this hybrid photodetector also extended the spectral response of perovskite photodetectors.

Photodetectors based on organic semiconductors (including small molecules and polymers) have received broad attention in recent years, which has led to a rapid development of organic solar cells and has involved the production of thousands of new semiconductor materials for tailored optoelectronic properties.[1–10] The low concentration of free carriers in organic semiconductors gives rise to low device noise, and the adoption of the bulk-heterojunction (BHJ) structure allows for the conversion of photons to electrons/holes at high efficiency, at levels close to unity. Both of these features contribute to the high detectivity levels of organic photodetectors, which are now comparable to the best photodetectors based on inorganic semiconductors. Benefiting from the rapid development of new polymeric materials, polymer-based photodetectors showing a wide spectral response, from the ultraviolet (UV) to the near infrared (NIR), have been produced.[6,7,11] Also, the ability to solution process these polymeric materials allows their direct patterning using ink-jet printing for imager arrays. However, the relatively slow response times of these materials limit the applications of polymer-based photodetectors. The low mobility values of free carriers in most polymeric materials (10^{-6}–10^{-1} cm^2 V^{-1} s^{-1})[12–14] impose limits on the maximum thickness of the organic BHJ layer. The photoactive films are generally made with a thickness of less than 150 nm so that they effectively collect the photogenerated free carriers in the BHJ layers even under large reverse bias. But such thin films inevitably show increased device capacitance due to the inverse relationship between capacitance and film thickness, which causes the device response time to be limited by the resistance–capacitance (RC) time constant of the devices. Although one could reduce the area of the device to enhance the speed of its response, the amount of light collected would then also be reduced. Most reported

[a] *Department of Mechanical and Materials Engineering, University of Nebraska–Lincoln, Lincoln, Nebraska 68588-0656, USA. E-mail: jhuang2@unl.edu*
[b] *Department of Electrical and Computer Engineering, University of Nebraska–Lincoln, Lincoln, Nebraska 68588-0656, USA*
[c] *Department of Physics and Astronomy, University of Nebraska–Lincoln, Lincoln, Nebraska 68588-0656, USA*
[d] *Institute of Chemistry, Chinese Academy of Sciences, 100190, China*
† Electronic supplementary information (ESI) available. See DOI: 10.1039/c6mh00508j
‡ L. S. and Y. L. contributed equally to this work.

polymer-based photodetectors with a device area larger than 0.1 mm^2 show a response time in the microsecond range, which corresponds to a response speed in the MHz range,[2,15,16] though the time-domain and frequency-domain responses cannot always be simply converted from one to the other. This tradeoff severely limits the further application of polymer-based photodetectors.

Organic–inorganic hybrid perovskites (OIHPs) have emerged as a new family of solution-processed semiconductor materials and have met with unprecedented success in solar cell development.[17–22] They show carrier mobility levels (1–250 $cm^2 V^{-1} s^{-1}$) several orders of magnitude greater than those of most polymers,[23–25] and these high levels allow for GHz response speeds of photodetectors based on pure perovskite, as we first demonstrated.[26] However, their response spectra have so far been reported to be limited to the UV-visible range below 800 nm.[27–29] Although the bandgap could be made to be in the NIR range by alloying the material with Sn, this resulting perovskite material is unstable in air due to the easy oxidation of Sn^{2+} to Sn^{4+}, which causes the perovskite to become metallic. Herein, we address the slow response time of organic photodetectors by integrating the OIHP with a low-bandgap polymer:fullerene BHJ layer to fabricate hybrid photodetectors that have a wide response spectrum ranging from 350 nm to 1050 nm, a directly measured Noise Equivalent Power (NEP) as low as 10.5 pW cm^{-2}, and an ultrafast response speed of 5 ns at a wavelength of 800 nm. To the best of our knowledge, this is the first polymer-based photodetector shown to achieve an approximately nanosecond scale response time.

The device structure shown in Fig. 1a was composed of indium tin oxide (ITO)/poly(bis(4-phenyl)(2,4,6-trimethylphenyl)amine) (PTAA)/$CH_3NH_3PbI_3$ ($MAPbI_3$)/poly{2,5-bis(2-hexyldecyl)-2,5-dihydropyrrolo[3,4-*c*]pyrrole-1,4-dione-3,6-di(5-thiophen-2-yl)yl-*alt*-*N*-(2-ethylhexyl)-dithieno-[3,2-*b*:2,3-*d*]pyrrole-2,6-diyl}:phenyl-C_{61}-butyric acid methyl ester (PDPPTDTPT:PCBM)/2,9-dimethyl-4,7-diphenyl-1,10-phenanthroline (BCP)/copper (Cu). PDPPTDTPT was measured here to have a low optical bandgap of 1.23 eV. Here, PTAA worked as non-wetting layers to increase the perovskite grain size and decrease the grain boundary area, which has been demonstrated in our previous reports and widely used in current work on perovskite photovoltaics.[22] The big perovskite grain size was also clearly observed in the cross-section of a scanning electron microscopy (SEM) image of the perovskite film on PTAA (Fig. 1b). Any of various PDPPTDTPT : PCBM blends (1 : *x*, *x* = 0, 1, 2, or 4) that we produced was made to directly contact $MAPbI_3$ instead of C_{60} or C_{60}/PCBM, and acted as a light-absorbing layer complementary to the perovskite layer. It was made to fully cover the perovskite layer, in order to avoid a direct injection of charge into the perovskite, which was important to reduce the dark current of the devices.

Fig. 1c shows a schematic energy diagram and working mechanism of the perovskite/polymer hybrid photodetector that we made. According to this mechanism, the UV-visible portion of light passing through the transparent ITO anode gets absorbed by the perovskite layer, with the NIR portion passing through the perovskite layer and being absorbed by the polymer blend layer. In this device structure, the perovskite layer according to this mechanism acts as a hole-transport layer for the BHJ layer, and the BHJ layer acts as an electron-transport layer for the perovskite layer. The holes generated in the BHJ layer by the NIR

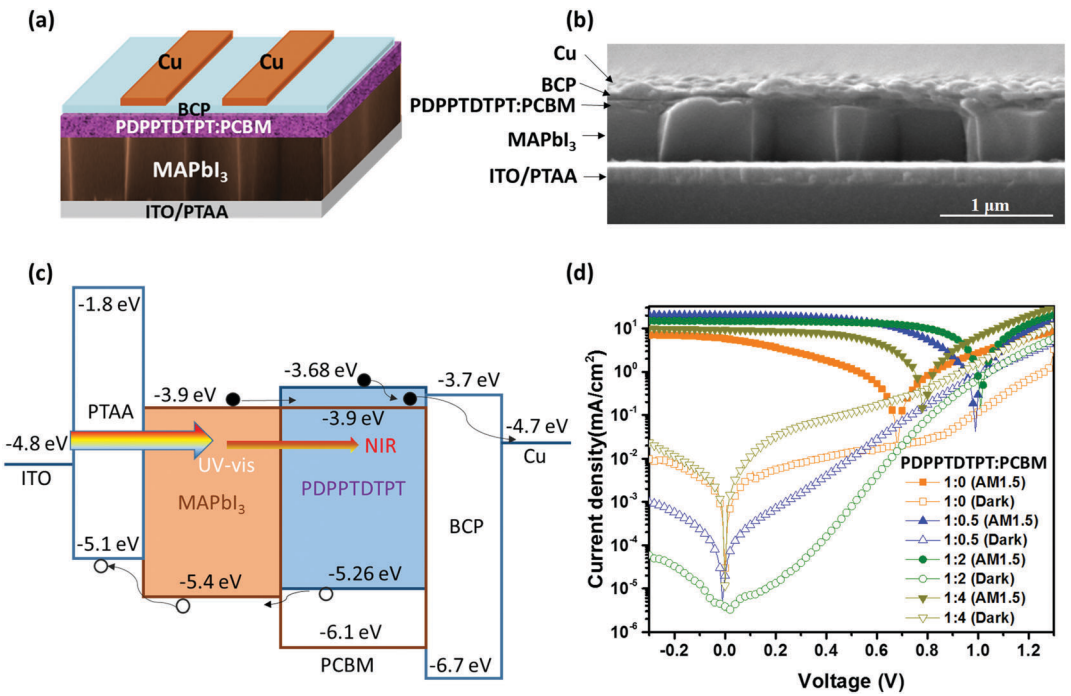

Fig. 1 (a) Schematic structure and (b) cross-section SEM image of the perovskite/polymer hybrid photodetector. (c) Schematic energy diagram of the perovskite/polymer hybrid photodetector. (d) Photocurrent and dark current curves of the perovskite/polymer hybrid photodetectors with various PDPPTDTPT : PCBM ratios.

light can be collected by the anode through the perovskite layer, with the photogenerated electrons directly collected by the cathode metal. The photogenerated electrons in the perovskite layer can also be successfully collected by the cathode after passing through the polymer blend layer, with the photogenerated holes directly collected by the anode. Despite a mismatch between the energy levels of the perovskite and the BHJ layer at their interface, holes and electrons have been demonstrated to transfer successfully between the perovskite and the polymer in perovskite/polymer solar cells.[30,31] This successful transfer may have been caused by the formation of interfacial dipoles or by a non-unified characterization of energy levels reported in the literature.

The device performance was shown to be sensitive to the ratio of the amounts of donor to acceptor in the BHJ layer. Fig. 1d displays the dark current and photocurrent density curves (under air mass 1.5 global illumination) of the perovskite/polymer hybrid photodetectors under bias ranging from −0.3 to 1.3 V. The dark current was found to be closely related to the mass ratio of PDPPTDTPT to PCBM. For the device with a PDPPTDTPT : PCBM mass ratio of 1 : 2, the dark current was measured to be as low as 8.7×10^{-5} mA cm^{-2}, under a bias of −0.3 V, which was at least one to two orders of magnitude lower than those of hybrid photodetectors with other PDPPTDTPT : PCBM ratios. The reduced dark current can be explained by the improved coverage of the perovskite film by the BHJ layer, which was revealed by the atomic force microscope (AFM) imaging shown in Fig. S1 (ESI†). The root-mean-square roughness gradually declined after attaching PDPPTDTPT : PCBM of various ratios with the top of the perovskite layer. The smoothness of the perovskite layer was found to increase when the relative amount of PCBM in the PDPPTDTPT:PCBM layer was increased. This observation can be explained by the increased thickness of the polymer blend layers with more PCBM. A better coverage of the perovskite layer would reduce the direct contact of perovskite with the metal electrode and thus reduce the dark current. Too much PCBM in the BHJ layer (PDPPTDTPT : PCBM with a mass ratio of 1 : 4), however, increased the dark current. This observation can be attributed to the worsened film morphology as well as the electron leakage through aggregated PCBM. The lower dark current is consistent with the results reported in our previous work, in which the C_{60} layer played an important role in decreasing the dark current.[26] This important role suggested that PDPPTDTPT : PCBM with an optimized ratio of its components can work analogously to a cathode buffer layer to reduce current injection. The dependence of the dark current on this ratio was in accordance with the reported dependence of the efficiency on the donor-to-acceptor ratio for PDPPTDTPT : PCBM-based solar cells, suggesting the optimized BHJ morphology and this ratio to be important in both cases to reduce leakage.

To determine the wavelength range of the response of the hybrid device, the external quantum efficiency (EQE) was measured at a bias of −0.2 V. As shown in Fig. 2a, the response wavelength was further extended to the NIR when the PDPPTDTPT:PCBM layer was incorporated with the perovskite layer. Benefiting from the light absorption capabilities of the BHJ blend layer, a peak EQE of ∼20% was obtained at a wavelength of 900 nm. The extended UV-visible-NIR response can be attributed to the structural design of the device, whose energy diagram is illustrated in Fig. 1c. For the PDPPTDTPT : PCBM mass ratio of 1 : 2, the EQE reached a maximum in the NIR wavelength range.

Low device dark current generally indicates a low noise current. In this work, to accurately obtain the noise current of the hybrid photodetectors with the lowest dark current, a fast Fourier transform (FFT) signal analyzer combined with a current pre-amplifier were used to directly record the noise currents at different frequencies. As shown in the inset of Fig. 2b, the noise current was as low as 3.48×10^{-13} A Hz$^{-1/2}$, and was insensitive to the frequency. This result indicated that the flicker noise induced by charge trapping did not dominate the total noise,[28] due to the passivation effect of the fullerene used in these devices.[32] Based on the directly measured noise current and responsivity, the specific detectivity (D^*) can be calculated and is shown in Fig. 2b. D^* was determined to be greater than 1×10^{11} cm Hz$^{1/2}$ W^{-1} at a wavelength of about 900 nm, leading to a calculated NEP of 5 pW cm^{-2}.

To further determine whether the photodetectors can actually detect NIR light intensity as low as this NEP and how large scopes the responsivity can keep constant, the signal current was directly measured under various light intensities with the FFT signal analyzer in the same way that the noise current was measured. The incident light from an NIR light-emitting diode (LED, electroluminescence peak at a wavelength of 890 nm) was modulated to 35 Hz by using an oscilloscope. As shown in Fig. 2c, a series of signal peaks appeared at 35 Hz as the irradiance decreased. When the light intensity decreased to below 10.5 pW cm^{-2}, the signal peak merged into the background noise and could no longer be differentiated from the noise current. The lowest measured light intensity was very close to the calculated NEP from D^*. We want to emphasize that it is very important to directly verify the NEP from experiment, rather than to derive it from the calculated D^*, as this D^* could be misleading since the responsivity is measured under strong light.

The linear dynamic range (LDR) of the photodetectors was measured with an LED whose emitted light had an average wavelength of 890 nm. The modulation frequency was chosen to be 35 Hz, which was consistent with the EQE measurement. As shown in Fig. 2d, the photocurrent density was clearly observed to increase linearly with increasing light intensity from about 10.0 pW cm^{-2} to 0.03 W cm^{-2}. This linear response of the device to changes in the light intensity over 9.5 orders of magnitude corresponded to a large LDR of 95 dB, which was found to be among the best results for perovskite and fullerene photodetectors.[27,28,33,34]

In addition to sensitivity, another important figure of merit for a photodetector is the response speed. Here, the response speed was measured by applying the transient photocurrent (TPC) method. The laser pulse was provided by a Ti–sapphire femtosecond (fs) laser with an emission wavelength of 800 nm, and involved doubling the frequency and pulse duration of 150 fs at a repeating frequency of 1 kHz. A short pulse of light from the femtosecond laser was used to generate carriers in the photodetectors that were driven toward the respective electrodes

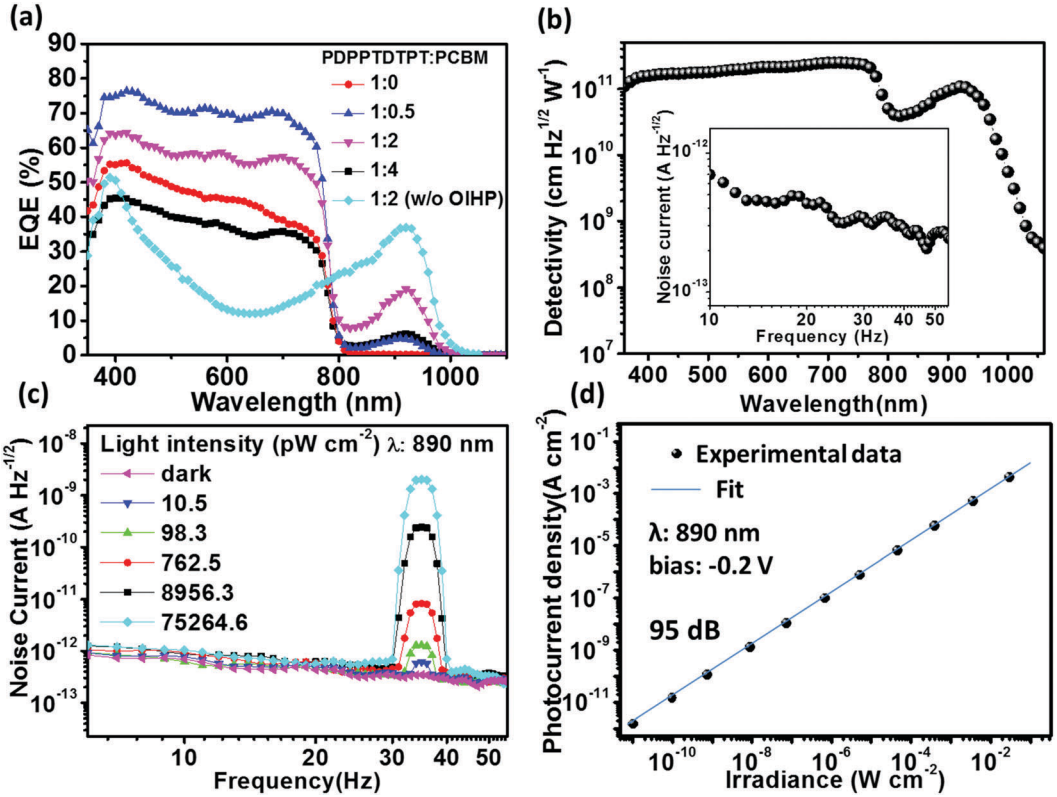

Fig. 2 (a) EQE values of perovskite/polymer hybrid photodetectors with different PDPPTDTPT : PCBM ratios, and that of the pure polymer (w/o OIHP) photodetector, at a bias of −0.2 V. (b) The specific detectivity values of the perovskite–polymer hybrid photodetector at various wavelengths of light under a bias of −0.1 V. Inset: The noise current of the photodetector at −0.1 V bias. (c) The noise currents of the perovskite/polymer hybrid photodetector in the dark and under illumination of various intensities of light with a wavelength of 890 nm. (d) The linear dynamic range of the perovskite/polymer hybrid under 890 nm-wavelength LED illuminations with various light intensities. The solid line is a linear fitting to the data. The photodetector was working at a bias of −0.2 V.

by the built-in potential field or an external voltage bias. The induced photocurrent pulse (or TPC curve) was recorded by using a fast oscilloscope with an input resistance of 50 Ω. By applying a single exponential fitting, the response speed can be defined from the linear regime extending out beyond the peak, all the way down to approximately the "1/*e*" time of the photocurrent decay. As shown in Fig. 3a, the response time of the perovskite/polymer hybrid photodetector with a 7 mm^2 area was determined to be about 88 ns by fitting the TPC curve decay. However, the response time of the polymer photodetector with the same area was about 168 ns (Fig. S2, ESI†), *i.e.*, twice as slow as that of the perovskite/polymer hybrid photodetector. Furthermore, the response time was further decreased to 6.1 ns when the device area of the perovskite/polymer hybrid photodetector was decreased to 0.1 mm^2.

For a p–i–n diode-type photodetector, the response time is mainly limited by two factors: the transit time of the carrier through the device and the RC of the device and the circuit. The transit time and the RC time constant of the device we produced with an area of 7 mm^2 were estimated to be 3.0 ns (Table S1, ESI†) and 147 ns (Table S2, ESI†), respectively. The detailed procedures used to calculate the transit time and RC time constant are shown in ESI.† The response speed for our devices was determined to be limited by the RC time constant. The fast response speed of the perovskite/polymer hybrid photodetector benefited from the inserted perovskite layer, which was able to reduce the capacitance of the whole device. The capacitance values measured for the devices (Fig. 3b) offered direct evidence of this effect. Fig. 3c shows the TPC curves of the perovskite/polymer hybrid photodetector in response to visible light (specifically at a wavelength of 525 nm). The response times of the devices with areas of 7 mm^2 and 0.1 mm^2 were 107 and 7.9 ns, respectively, which were slightly slower than that to NIR light. This result can be explained by the lower mobility of electrons than of holes in perovskite.[24] When the devices were excited by visible light, the charge carriers were mainly generated in the perovskite layer due to its large absorption coefficient in the visible-wavelength range. The photogenerated electrons moved through the perovskite and BHJ layers before they were collected by the cathode. When the devices were excited by NIR light, the charge carriers were mainly generated in the polymer layer, and the photo-generated holes moved through the perovskite layer before they were collected by the anode. The response time of the devices to UV light was slightly longer than that to the other wavelengths (Fig. S3, ESI†), which was in accordance with this scenario. Fig. 3d shows the response time of the perovskite/polymer hybrid photodetector to visible light as a function of device area. The response time decreased linearly with the device

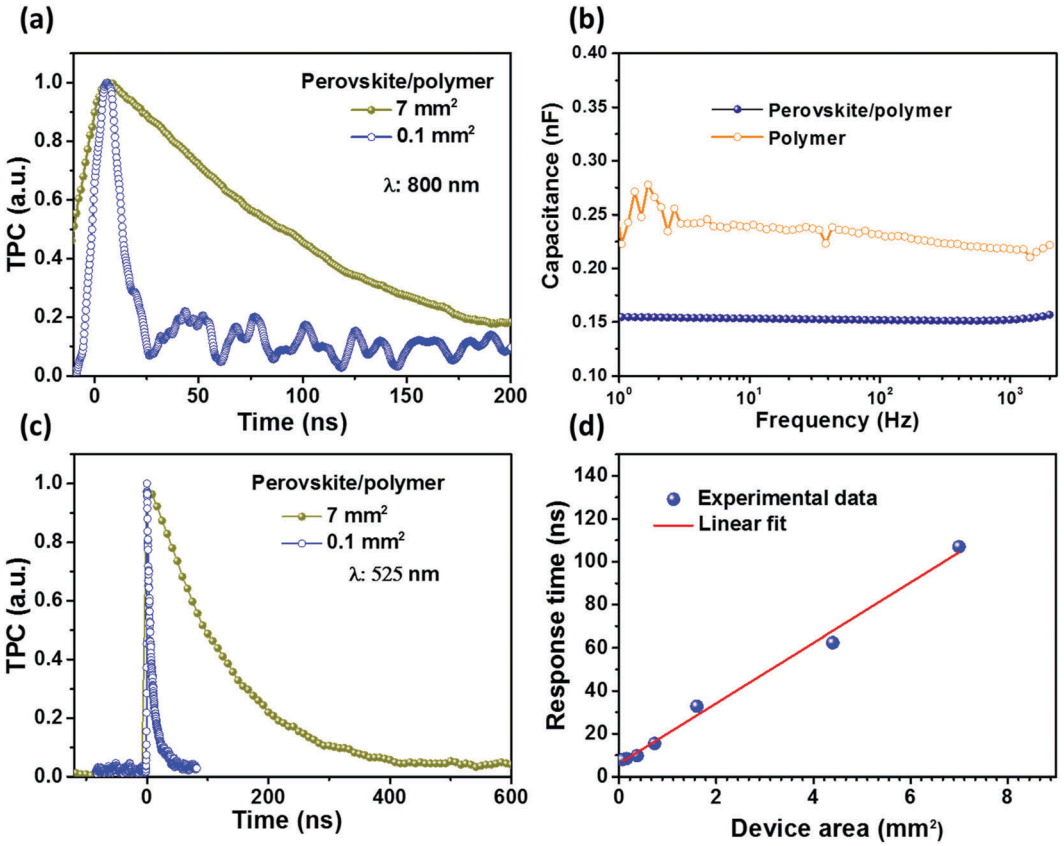

Fig. 3 (a) Transient photocurrent (TPC) curves of the perovskite/polymer hybrid photodetectors with device areas of 7 mm^2 and 0.1 mm^2 under illumination of near infrared light (specifically with a wavelength of 800 nm); the response time of devices with these two areas were determined to be 88 and 6.1 ns, respectively. (b) Capacitance values of the perovskite/polymer hybrid photodetector and the pure polymer photodetector measured for various frequencies. (c) TPC curves of the perovskite/polymer hybrid photodetectors with the device areas of 7 and 0.1 mm^2 under the illumination of visible light (specifically with a wavelength of 525 nm); the response times of the hybrid photodetectors with these two areas were 107 and 7.9 ns, respectively. (d) Measured response times of the perovskite/polymer hybrid photodetector for various device areas. The red line is the linear fit to the experiment data.

area, which confirmed that the response speed of the perovskite/polymer hybrid photodetector was mainly limited by the RC time constant.

The $MAPbI_3$ layer was measured in the current investigation to have a low photoresponse to light at a wavelength of 800 nm, which we attributed to its weak absorption of this light. Because of this low photoresponse, it was difficult to determine whether the ultrafast response time of ~6 ns arose from the perovskite layer or the polymer–fullerene blend layer. To accurately demonstrate the origin of the NIR response, $MAPbI_xBr_{3-x}$ was

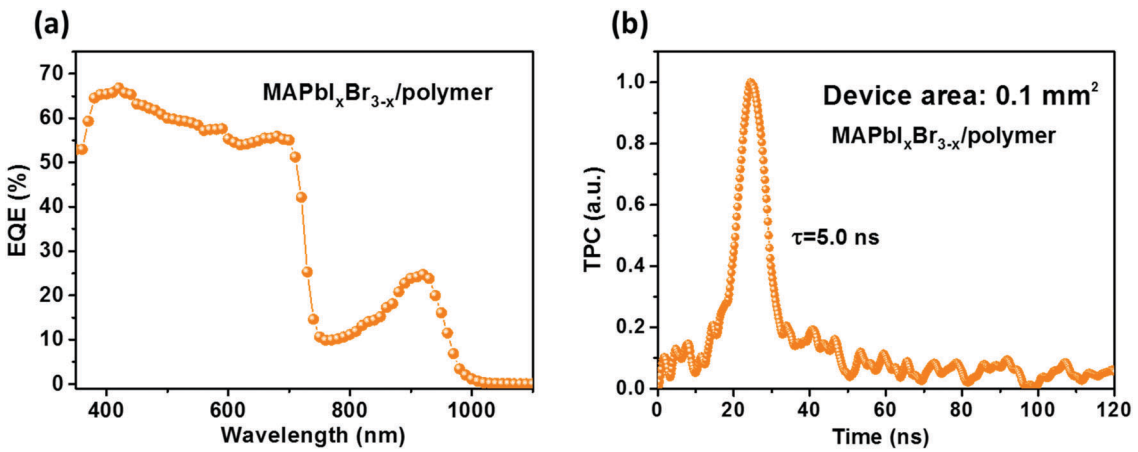

Fig. 4 (a) EQE of the $MAPbI_xBr_{3-x}$/polymer hybrid photodetector. (b) TPC curve of the $MAPbI_xBr_{3-x}$/polymer hybrid photodetector with a device area of 0.1 mm^2. The TPC lifetime of the device was found to be 5.0 ns.

used to replace $MAPbI_3$ to blue-shift the absorption cutoff to the wider bandgap. The absorption cutoff wavelength of the $MAPbI_xBr_{3-x}$ applied here was 740 nm, as shown in Fig. 4a, indicating that the NIR absorption of these devices completely came from the BHJ layer. By fitting the TPC curve of the $MAPbI_xBr_{3-x}$-based NIR photodetector, a comparable response time of 5 ns was obtained, as shown in Fig. 4b. This result provided direct evidence that an NIR detector can achieve an ultrafast response.

In summary, by integrating the perovskite and polymer BHJ into a single device, we fabricated a low-noise photodetector displaying ultrafast responses to a broad (UV-to-NIR) spectrum of light. The hybrid device showed an external quantum efficiency of 55–65% in the wavelength range 350 nm to 800 nm, and 10–20% in the wavelength range 800 nm to 950 nm. Moreover, for NIR light detection, the perovskite layer acted as the hole-transport layer, which enlarged the spacing of the two electrodes, decreased the device capacitance, and reduced the device response time to 5 ns. To the best of our knowledge, this is the fastest reported polymer-based photodetector with the device area tested.

Experimental section

Device fabrication

Patterned ITO glass was washed with acetone and 2-propanol in an ultrasonic bath three times, respectively, and then treated with UV-ozone for 30 min. A PTAA toluene solution was coated onto clean ITO substrates by spin coating at a speed of 5000 rpm and then annealing at 100 °C for 10 min. PbI_2 and CH_3NH_3I (MAI) were dissolved in dimethylformamide (DMF) and 2-propanol with concentrations of 630 mg ml^{-1} and 65 mg ml^{-1}, respectively. The PbI_2 solution was spun on the PTAA layer at 6000 rpm for 35 s and then dried at 90 °C on a hot plate. The MAI solution was spun on the PbI_2 film at 6000 rpm for 35 s. The perovskite film was obtained by annealing the stacked layers at 100 °C for 1 h on the hot plate. A blend of PDPPTDTPT with PCBM (PDPPTDTPT: 1.5 mg ml^{-1}) was dissolved in a mixed solution of chloroform and 1,2-dichlorobenzene (95 : 5 v/v) and then spun on the perovskite film at 1000 rpm for 60 s to form a photoactive BHJ layer. Finally, fabrication of the device was completed by thermally evaporating BCP (8 nm) and Cu (80 nm) sequentially.

Device characterization

J–V curves of the devices in the dark and under illumination were acquired based on measurement made with a Keithley 2400 source meter. The incident light was from a Xenon-lamp-based solar simulator (Oriel 67005, 150 W) that was calibrated to AM1.5G (100 mW cm^{-2}) by a silicon photodiode (Hamamatsu S1133). The external quantum efficiency (EQE) values of the devices were measured using a Newport QE measurement system. When collecting the photocurrent signal, the incident monochromatic light was modulated to 35 Hz with a chopper. When characterizing the TPC curves, all of the cables that connected the device and oscilloscope needed to be as short as possible; the device and oscilloscope were connected with a fast (6 GHz) Bayonet Neill–Concelman (BNC) connector to minimize the influence of the inductance of the circuit. The oscilloscope was turned on by the laser signal to record the TPC curve.

Acknowledgements

This work was supported by Department of Homeland Security under Award No. 2014-DN-077-ARI069-02, Defense Threat Reduction Agency HDTRA1-10-1-0098 and National Science Foundation under award ECCS-1348272. Huang and Lu also thank the financial support from Nebraska Center for Energy Sciences Research.

References

1 H. Dong, H. Zhu, Q. Meng, X. Gong and W. Hu, *Chem. Soc. Rev.*, 2012, **41**, 1754.
2 J. Clark and G. Lanzani, *Nat. Photonics*, 2010, **4**, 438.
3 F. Guo, B. Yang, Y. Yuan, Z. Xiao, Q. Dong, Y. Bi and J. Huang, *Nat. Nanotechnol.*, 2012, **7**, 798.
4 P. Peumans, V. Bulovic and S. R. Forrest, *Appl. Phys. Lett.*, 2000, **76**, 3855.
5 G. A. O'Brien, A. J. Quinn, D. A. Tanner and G. Redmond, *Adv. Mater.*, 2006, **18**, 2379.
6 D. Ray and K. L. Narasimhan, *Appl. Phys. Lett.*, 2007, **91**, 093516.
7 S. H. Wu, W. L. Li, B. Chu, C. S. Lee, Z. S. Su, J. B. Wang, F. Yan, G. Zhang, Z. Z. Hu and Z. Q. Zhang, *Appl. Phys. Lett.*, 2010, **96**, 093302.
8 H.-Y. Chen, M. K. F. Lo, G. Yang, H. G. Monbouquette and Y. Yang, *Nat. Nanotechnol.*, 2008, **3**, 543.
9 R. Dong, C. Bi, Q. Dong, F. Guo, Y. Yuan, Y. Fang, Z. Xiao and J. Huang, *Adv. Opt. Mater.*, 2014, **2**, 549.
10 S. F. Tedde, J. Fu, M. V. Kovalenko, T. Rauch, M. Bo, U. Lemmer, W. Heiss and O. Hayden, *Nat. Photonics*, 2009, **3**, 332.
11 J. D. Zimmerman, V. V. Diev, K. Hanson, R. R. Lunt, E. K. Yu, M. E. Thompson and S. R. Forrest, *Adv. Mater.*, 2010, **22**, 2780.
12 Z. Bao, A. Dodabalapur and A. J. Lovinger, *Appl. Phys. Lett.*, 1996, **69**, 4108.
13 H. Sirringhaus, N. Tessler and R. H. Friend, *Science*, 1998, **280**, 1741.
14 H. Sirringhaus, P. J. Brown, R. H. Friend, M. M. Nielsen, K. Bechgaard, B. M. W. Langeveld-Voss, A. J. H. Spiering, R. A. J. Janssen, E. W. Meijer, P. Herwig and D. M. de Leeuw, *Nature*, 1999, **401**, 685.
15 S. Tay, J. Thomas, M. Eralp, G. Li, R. A. Norwood, A. Schülzgen, M. Yamamoto, S. Barlow, G. A. Walker, S. R. Marder and N. Peyghambarian, *Appl. Phys. Lett.*, 2005, **87**, 1.
16 L. Salamandra, G. Susanna, S. Penna, F. Brunetti and A. Reale, *IEEE Photonics Technol. Lett.*, 2011, **23**, 780.
17 M. Lee, J. Teuscher, T. Miyasaka, T. N. Murakami and H. J. Snaith, *Science*, 2012, **338**, 643.
18 H.-S. Kim, C.-R. Lee, J.-H. Im, K.-B. Lee, T. Moehl, A. Marchioro, S.-J. Moon, R. Humphry-Baker, J.-H. Yum, J. E. Moser, M. Gratzel and N.-G. Park, *Sci. Rep.*, 2012, 591.

19 M. Liu, M. B. Johnston and H. J. Snaith, *Nature*, 2013, **501**, 395.
20 A. Mei, X. Li, L. Liu, Z. Ku, T. Liu, Y. Rong, M. Xu, M. Hu, J. Chen, Y. Yang, M. Gratzel and H. Han, *Science*, 2014, **345**, 295.
21 Q. Dong, J. Song, Y. Fang, Y. Shao, S. Ducharme and J. Huang, *Adv. Mater.*, 2016, **28**, 2816.
22 C. Bi, Q. Wang, Y. Shao, Y. Yuan, Z. Xiao and J. Huang, *Nat. Commun.*, 2015, **6**, 7747.
23 C. C. Stoumpos, C. D. Malliakas and M. G. Kanatzidis, *Inorg. Chem.*, 2013, **52**, 9019.
24 Q. Dong, Y. Fang, Y. Shao, P. Mulligan, J. Qiu, L. Cao and J. Huang, *Science*, 2015, **347**, 967.
25 H. Oga, A. Saeki, Y. Ogomi, S. Hayase and S. Seki, *J. Am. Chem. Soc.*, 2014, **136**, 13818.
26 L. Shen, Y. Fang, D. Wang, Y. Bai, Y. Deng, M. Wang, Y. Lu and J. Huang, *Adv. Mater.*, 2016, **28**, 10794.
27 L. Dou, Y. (Micheal) Yang, J. You, Z. Hong, W.-H. Chang, G. Li and Y. Yang, *Nat. Commun.*, 2014, **5**, 5404.
28 Y. Fang and J. Huang, *Adv. Mater.*, 2015, **27**, 2804.
29 Y. Fang, Q. Dong, Y. Shao, Y. Yuan and J. Huang, *Nat. Photonics*, 2015, **9**, 679.
30 C. Zuo and L. Ding, *J. Mater. Chem. A*, 2015, **3**, 9063.
31 Y. Liu, Z. Hong, Q. Chen, W. Chang, H. Zhou, T.-B. Song, E. Young, Y. (Michael) Yang, J. You, G. Li and Y. Yang, *Nano Lett.*, 2015, **15**, 662.
32 Y. Shao, Z. Xiao, C. Bi, Y. Yuan and J. Huang, *Nat. Commun.*, 2014, **5**, 5784.
33 Q. Lin, A. Armin, D. M. Lyons, P. L. Burn and P. Meredith, *Adv. Mater.*, 2015, **27**, 2060.
34 F. Guo, Z. Xiao and J. Huang, *Adv. Opt. Mater.*, 2013, **1**, 289.

